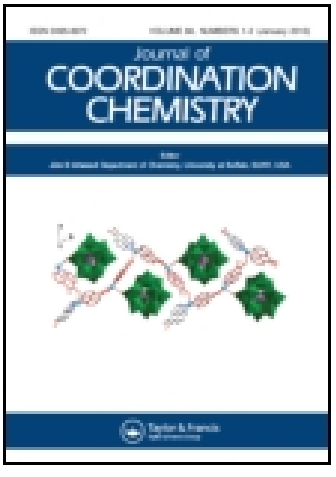

Journal of Coordination Chemistry
Publication details, including instructions for authors and subscription information:
http://www.tandfonline.com/loi/gcoo20

Synthesis, structures, and fluorescent properties of azo anthranilic acid and its Cu(II), Co(II), and Ni(II) complexes

Yong-Feng Qiao[ab], Lin Du[a], Jie Zhou[a], Yan Hu[a], Lin Li[a], Bin Li[a] & Qi-Hua Zhao[a]

[a] School of Chemical Science and Technology, Yunnan University, Kunming, China

[b] Department of Chemical Science and Technology, Kunming University, Kunming, China

Accepted author version posted online: 29 Jul 2014.Published online: 26 Aug 2014.

To cite this article: Yong-Feng Qiao, Lin Du, Jie Zhou, Yan Hu, Lin Li, Bin Li & Qi-Hua Zhao (2014) Synthesis, structures, and fluorescent properties of azo anthranilic acid and its Cu(II), Co(II), and Ni(II) complexes, Journal of Coordination Chemistry, 67:15, 2615-2629, DOI: 10.1080/00958972.2014.948870

To link to this article: http://dx.doi.org/10.1080/00958972.2014.948870

Journal of Coordination Chemistry, 2014
Vol. 67, No. 15, 2615–2629, http://dx.doi.org/10.1080/00958972.2014.948870

Synthesis, structures, and fluorescent properties of azo anthranilic acid and its Cu(II), Co(II), and Ni(II) complexes

YONG-FENG QIAO†‡, LIN DU†, JIE ZHOU†, YAN HU†, LIN LI†, BIN LI† and QI-HUA ZHAO*†

†School of Chemical Science and Technology, Yunnan University, Kunming, China
‡Department of Chemical Science and Technology, Kunming University, Kunming, China

(*Received 27 March 2014; accepted 26 June 2014*)

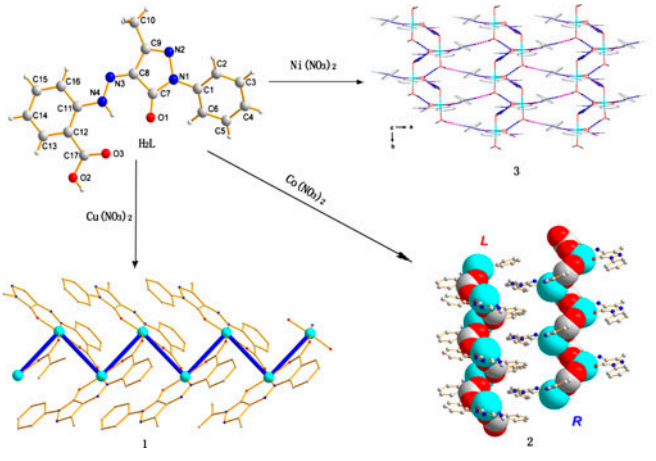

Three new complexes, $[Cu(II)L]_n$ (**1**), $[Co(II)L(H_2O)]_n$ (**2**), and $[Ni(II)L(DMF)(H_2O)_2]$ (**3**), where H_2L = [2-(2-(3-methyl-5-oxo-1-phenyl-1H-pyrazol-4(5H)-ylidene) hydrazinyl) benzoic acid], were synthesized and characterized via elemental analysis, IR spectroscopy, and single-crystal X-ray diffraction. Single-crystal X-ray diffraction analysis revealed that **1**, **2**, and **3**, formed by H_2L with metal nitrate, have zigzag chain, helical chain, and mononuclear structures, respectively. The luminescence spectra study reveals that **1** has two emission peaks at 470 and 540 nm, which are attributed to intraligand charge transfer and ligand-to-metal charge transfer fluorescent emission, respectively. In **2** and **3**, almost 100% fluorescence emission quenching is observed.

Keywords: Azo anthranilic; Coordination polymer; Crystal structure; Thermal property; Fluorescent property

1. Introduction

Coordination polymers, which have potential applications in fields such as magnetic materials and luminescence, have received considerable attention [1–4]. Their structural

*Corresponding author. Email: qhzhao@ynu.edu.cn

diversities can be influenced by numerous controlled and accidental factors, such as structure of the organic ligand, metal ion and coordination possibilities, reaction temperature, and solvent [5–9]. Several critical factors in the design and synthesis of desirable coordination polymers include the rational design and synthesis of multidentate ligands [10–12].

Increasing research has focused on the theoretical and applied fluorescent chemisensors with potential analytical applications in chemistry and biology [13–17]. As an important class of compounds, azo compounds and their complexes, which possess good optical characteristics, are of interest not only for application in dyes, but also for photometric analysis, non-linear optics, and optical information storage [18–21]. Similar UV–vis spectra of the complexes of azo ligands with Cu(II), Co(II), and Ni(II) have been found, which renders the detection of one from the other two ions via UV–vis absorption spectroscopy difficult [22, 23]. Fluorescence may provide a method to solve this problem with fluorescence analysis.

From the structure of 2-(2-(3-methyl-5-oxo-1-phenyl-1H-pyrazol-4(5H)-ylidene) hydrazinyl), benzoic acid (H_2L) has coordination features of both 4-acyl-1-phenyl-5-pyrazolones and anthranilic acid. Two unsymmetrical oxygen donors are found in compounds of 4-acyl-1-phenyl-5-pyrazolone, which form a class of unsymmetrical β-diketone compounds and can chelate transition, and rare metal earth ions [24–28]. Most of these ligands form zero-dimensional compounds by losing a proton of the enol giving only two donors and a mono negative ligand. To generate polymers, Jia *et al.* used 4,4′-bipyridine as a bridging ligand that links two adjacent units, thereby resulting in the formation of an infinite 1-D zigzag chain structure [29]. Recently, the group synthesized several polymers by introducing more donors in the Schiff base derivatives of 4-acyl-5-pyrazolones [30]. Their study provided a new approach to obtain more polymers composed of pyrazolone derivatives.

Carboxyl groups can function as linkers between metal ions for propagation of metal–ligand coordination units because of their divergent bridging capabilities. During the formation of coordination polymers, carboxyl groups have numerous types of bridging conformations. The most common ones are triatomic *syn–syn*, *syn–anti*, and *anti–anti* [31–33]. In our previous work [34, 35], several coordination polymers with novel structures were synthesized, and the carboxyl groups exhibited flexible coordination modes. To maintain the chelating ability of H_2L and to increase its coordination flexibility, we used the compound as the main ligand, which had more potential donors than 4-acyl-1-phenyl-5-pyrazolones. Taking into account the impact of structure on optical properties, we present the synthesis, structures, and properties of H_2L and its complexes, $[Cu(II)L]_n$ (**1**), $[Co(II)L{\cdot}H_2O]_n$ (**2**), and $Ni(II)L(DMF)(H_2O)_2$ (**3**), in this article.

2. Experimental

2.1. *General*

All reagents were of analytical grade and used as received. Double-deionized water was used in all of the syntheses. Elemental analyses for C, H, and N were performed using a Vario-EL III element analyzer. The samples were pressed as KBr pellets, and Fourier transform IR spectra were recorded using a SHIMADZU IR prestige-21 FTIR-8400S spectrometer from 4000 to 400 cm^{-1}. The phase purity of the samples was investigated via powder X-ray diffraction (PXRD) carried out using a Bruker D8-Advance diffractometer with Cu-Kα radiation (λ = 1.5406 Å) at a scan speed of 1° min^{-1}. PXRD pattern simulations were performed using single-crystal data and processed using the Mercury v1.4 program,

which is available free of charge at http://www.iucr.org. The crystal structures were determined using a Rigaku SCXmini diffractometer and the SHELXL-97 crystallographic software package. Thermogravimetric analysis (TGA) data were collected using a simultaneous SDT thermal analyzer at a heating rate of 10 °C min^{-1} under a N_2 atmosphere (N_2 flow rate = 0.03 L min^{-1}). The solid-state fluorescence spectra were studied at room temperature using a Hitachi FL-7000 fluorescence spectrophotometer with excitation and emission slit widths of 5 nm.

2.2. *Preparation of H_2L*

H_2L was prepared according to a modified method [36]: anthranilic acid (1.37 g, 0.01 M) and sodium nitrite (0.69 g, 0.01 M) were mixed in 20 mL of double-deionized water, cooled to 0–5 °C, and then added with hydrochloric acid with vigorous stirring. The so-formed diazonium salt solution was then coupled with the cooled solution of 3-methyl-1-phenyl-pyrazol-5-one (1.74 g, 0.01 M) at pH 9 and 10. The orange–red precipitate was filtered off and recrystallized from glacial acetic acid, which resulted in an 81% yield (based on anthranilic acid) of orange needle-like crystals. These crystals were soluble in DMSO, methanol, ethanol, chloroform, and glacial acetic acid. Anal. Calcd for [H_2L] (%): C, 63.35; N, 17.38; H, 4.38. Found (%): C, 63.61; N, 17.65; H, 4.41. IR (KBr, cm^{-1}): 3432, 3066, 3014, 2924, 1671, 1664, 1603, 1583, 1541, 1500, 1452, 1342, 1274, 1240, 1165, 1049, 1000, 762, 679, 577, and 461.

2.3. *Preparation of $[Cu(II)L]_n$ (1)*

A mixture of H_2L (96.6 mg, 0.3 mM) and $Cu(NO_3)_2{\cdot}6H_2O$ (72.5 mg, 0.3 mM) was dissolved in a mixed ethanol–DMF solution (v : v = 1 : 1, 10.0 mL). NaOH (24 mg, 0.6 mM) was added dropwise into the above mixture. The solution was stirred for 2 h at 80 °C and filtered into a sealed beaker. After a month, black block-shaped crystals were obtained and washed several times with ethanol. The following values were noted: Yield: 64% based on Cu^{II}. Anal. for $[Cu(II)L]_n$ (**1**) (%): C, 53.19; N, 14.59; H, 3.15. Found (%): C, 53.56; N, 14.81; H, 3.19. IR (KBr, cm^{-1}): 3072, 2928, 1582, 1542, 1496, 1450, 1301, 1255, 1240, 1158, 1042, 1004, 885, 755, 700, 594, and 454.

2.4. *Preparation of $[Co(II)L(H_2O)]_n$ (2)*

H_2L (96.6 mg, 0.3 mM) and $Co(NO_3)_2{\cdot}6H_2O$ (87.3 mg, 0.3 mM) were dissolved in ethanol (10.0 mL). NaOH (24 mg, 0.6 mM) was added dropwise into the above mixture and the mixture was allowed to stand at room temperature. The solution was stirred for 30 min at ambient temperature and then filtered. Regular dark-red, block-shaped crystals were obtained after 10 days. These crystals were washed several times with ethanol and water, and then dried in vacuum. The following values were noted. Yield: 71% based on Co^{II}. Anal. for $[Co(II)L(H_2O)]_n$ (**2**) (%): C, 51.40; N, 14.10; H, 3.55. Found (%): C, 51.38; N, 14.43; H, 3.61. IR (KBr, cm^{-1}): 3233, 3068, 2921, 1592, 1559, 1487.27, 1418, 1391, 1335, 1301, 1261, 1212, 1063, 1008, 750, 724, 700, 588, 509, and 437.

2.5. *Preparation of $[Ni(II)L(DMF)(H_2O)_2]$ (3)*

H_2L (96.6 mg, 0.3 mM) and $Ni(NO_3)_2{\cdot}6H_2O$ (87.2 mg, 0.3 mM) were mixed and dissolved in ethanol–DMF solution (v : v = 1 : 1, 10.0 mL). NaOH (24 mg, 0.6 mM) was added

Table 1. Crystal and structure refinement data for H_2L and **1–3**.

	H_2L	**1**	**2**	**3**
Empirical formula	$C_{17}H_{14}N_4O_3$	$C_{17}H_{12}CuN_4O_3$	$C_{17}H_{14}CoN_4O_4$	$C_{20}H_{23}N_5NiO_6$
Formula weight	322.32	383.85	397.25	488.14
Crystal system	Monoclinic	Monoclinic	Tetragonal	Monoclinic
Space group	*P2(1)/c*	*C2/c*	$I\bar{4}$	*P2(1)/c*
a (Å)	7.0560(9)	30.533(6)	21.8869(15)	11.3392(15)
b (Å)	18.562(2)	6.1764(12)	21.8869(15)	7.4073(10)
c (Å)	11.5301(14)	19.347(4)	7.1458(10)	26.086(3)
α (°)	90	90	90	90
β (°)	94.839(2)	122.047(2)	90	105.734(5)
γ (°)	90	90	90	90
V (Å^3)	1504.7(3)	3092.5(11)	3423.1(6)	2108.9(5)
Z	4	8	8	4
Calcd density (mg m^{-3})	1.423	1.649	1.542	1.537
Absorption coefficient (mm^{-1})	0.101	1.438	1.034	0.969
R_{int}	0.1017	0.0715	0.0661	0.0726
R_1 [$I > 2\sigma(I)$]	0.0500	0.0547	0.0510	0.0537
ωR [$I > 2\sigma(I)$]	0.0791	0.1025	0.1075	0.1177
Goodness-of-fit on F^2	0.998	0.984	1.041	1.033
Residuals (e Å^{-3})	0.194, −0.248	0.445, −0.431	0.425, −0.387	0.628, −0.511

dropwise into the above mixture. The solution was heated until the solvent evaporated. The residue was dissolved in 10.0 mL of ethanol and then filtered. Regular black block-shaped crystals were obtained after 8 days. These crystals were washed several times with ethanol and water, and then dried in vacuum. The following values were noted: Yield: 45% based on Ni^{II}. Anal. for [Ni(II)L(DMF)(H_2O)$_2$] (**3**) (%): C, 49.17; N, 14.34; H, 4.75. Found (%): C, 49.45; N, 14.62; H, 4.78. IR (KBr, cm^{-1}): 3440, 2924, 1603, 1493, 1421, 1324, 1182, 1118, 755, 604, and 461.

2.6. *Crystallographic data collection and refinement*

Selected single crystals of H_2L, **1**, **2**, and **3** with suitable dimensions were mounted on a glass fiber and used for the X-ray diffraction analyses. Crystallographic data were collected at 293 K using a Bruker Smart AXS CCD diffractometer with graphite-monochromated Mo-Kα radiation (λ = 0.71073 Å). Empirical absorption corrections were carried out using SADABS [37]. The structures were solved using direct methods and then refined on F^2 via the full-matrix least-squares technique using SHELXL-97. SHELXS-97 and SHELXL-97 were used for structure solution and refinement [38, 39]. All non-hydrogen atoms were refined with anisotropic displacement parameters. All of the hydrogens of the organic ligand were located using geometrical considerations and then refined isotropically with fixed U values via a riding model. The details on crystallographic data collection and refinement parameters are summarized in table 1. Selected bond distances and angles of H_2L, **1**, **2**, and **3** are listed in table 2. Hydrogen bonds are listed in table 3.

3. Results and discussion

3.1. *Spectral investigation*

Marked differences were observed in IR spectra of the complexes and free ligand (figure S1, see online supplemental material at http://dx.doi.org/10.1080/00958972.2014.948870).

Table 2. Selected bond lengths (Å) and angles (°) for H_2L and **1–3**.

H_2L			
O(1)–C(7)	1.2350(16)	C(7)–C(8)	1.462(2)
N(3)–C(8)	1.3093(18)	N(3)–N(4)	1.3253(15)
O(2)–C(17)	1.2214(16)	O(3)–C(17)	1.3054(16)
Complex **1**			
O(1)–C(7)	1.265(5)	C(7)–C(8)	1.420(5)
N(3)–C(8)	1.327(5)	N(3)–N(4)	1.291(4)
O(2)–C(17)	1.269(5)	O(3)–C(17)	1.254(5)
Cu(1)–O(2)#1	1.886(3)	Cu(1)–O(1)#1	1.916(3)
Cu(1)–O(3)	1.973(3)	Cu(1)–N(4)#1	1.984(3)
O(2)#1–Cu(1)–O(1)#1	170.37(11)	O(3)–Cu(1)–N(4)#1	175.98(14)
O(2)#1–Cu(1)–O(3)	83.34(12)	O(1)#1–Cu(1)–O(3)	87.13(12)
O(2)#1–Cu(1)–N(4)#1	93.26(13)	O(1)#1–Cu(1)–N(4)#1	96.32(12)
Complex **2**			
O(1)–C(7)	1.272(6)	C(7)–C(8)	1.424(7)
N(3)–C(8)	1.362(6)	N(3)–N(4)	1.299(5)
O(2)–C(17)	1.274(6)	O(3)–C(17)	1.242(6)
Co(1)–O(2)#1	1.960(4)	Co(1)–O(1)#1	1.956(3)
Co(1)–O(3) #1	2.111(3)	Co (1)–N(4)	2.103(4)
Co(1)–O(4)	2.011(4)		
O(1)–Co(1)–O(2)	130.27(19)	O(1)–Co(1)–O(4)	113.17(19)
O(2)–Co(1)–O(4)	116.38(19)	O(1)–Co(1)–N(4)	91.49(15)
O(2)–Co(1)–N(4)	88.01(15)	O(4)–Co(1)–N(4)	95.28(16)
O(1)–Co(1)–O(3)#1	87.01(13)	O(2)–Co(1)–O(3)#1	86.50(15)
O(4)–Co(1)–O(3)#1	93.11(16)	N(4)–Co(1)–O(3)#1	171.38(17)
Complex **3**			
O(1)–C(7)	1.265(5)	C(7)–C(8)	1.429(6)
N(3)–C(8)	1.345(5)	N(3)–N(4)	1.301(4)
O(2)–C(17)	1.272(5)	O(3)–C(17)	1.237(5)
Ni–O(2)	1.974(3)	Ni–O(1)	1.981(3)
Ni–N(4)	2.036(3)	Ni–O(6)	2.098(3)
Ni–O(4)	2.099(3)	Ni–O(5)	2.100(3)
O(2)–Ni–O(1)	169.13(11)	O(2)–Ni–N(4)	91.64(12)
O(1)–Ni–N(4)	96.62(12)	O(2)–Ni–O(6)	83.54(11)
O(1)–Ni–O(6)	88.76(11)	N(4)–Ni–O(6)	173.33(11)
O(2)–Ni–O(4)	97.72(11)	O(1)–Ni–O(4)	89.55(11)
N(4)–Ni–O(4)	88.67(13)	O(6)–Ni–O(4)	87.42(12)
O(2)–Ni–O(5)	88.55(11)	O(1)–Ni–O(5)	84.12(11)
N(4)–Ni–O(5)	91.98(12)	O(6)–Ni–O(5)	92.50(12)
O(4)–Ni–O(5)	173.68(11)		

Notes: Symmetry transformations used to generate equivalent atoms for **1**: #1 $-x+3/2$, $y+1/2$, $-z+3/2$; #2 $-x+3/2$, $y-1/2$, $-z+3/2$; for **2**: #1 $-x+1/2$, $-y+1/2$, $z-1/2$; #2 $-x+1/2$, $-y+1/2$, $z+1/2$.

IR spectra of H_2L exhibit one medium-intensity broad band at 2700–3250 cm^{-1}, which can either be assigned to the two O–H for the tautomeric enol-azo form (scheme 1) or N–H and O–H for the hydrazone form (scheme 1). This band is assigned to N–H and O–H for the latter form based on the information obtained from crystallographic studies. In IR spectra of the complexes, the N–H and O–H stretches disappeared, indicating deprotonation of N–H and carboxyl groups (–COOH) in the metal complexes. Two strong bands around 1671 and 1664 cm^{-1} were present for free HL, due to the (C=O) of the pyrazolone ring and carboxyl group, respectively, but were absent in **1** and **2**. The broad peak at 1603 cm^{-1} in **3**, which possibly corresponds to peaks of carbonyl of DMF and carboxyl group, can be assigned to the phenyl ring based on its crystal structure. From the above analysis, we conclude that the enolic protons of ligand are replaced by Cu(II), Co(II), and Ni(II) in **1**, **2**, and **3**, respectively.

Table 3. Hydrogen bonds of H_2L, **2** and **3**.

D–H…A	d(D–H) (Å)	d(H…A) (Å)	d(D…A) (Å)	(D–H…A) (°)
H_2L				
N(4)–H(1A)…O(1)	0.876(16)	2.110(17)	2.7937(16)	134.3(13)
N(4)–H(1A)…O(2)	0.876(16)	2.064(15)	2.6997(15)	128.7(13)
O(3)–H(2B)…O(2)#1	0.82	1.82	2.6373(15)	173
Complex **2**				
O(1)–H(1)…O(2)#2	0.82	1.97	2.701(5)	148
O(1)–H(1B)…N(3)#3	0.72(9)	2.03(9)	2.752(5)	174(9)
Complex **3**				
O(5)–H(5A)…O(6)#4	0.82	2.22	2.995(3)	158
O(5)–H(5B)…O(3)#4	0.95(4)	1.97(4)	2.916(4)	172(4)
O(4)–H(4A)…N(2)#5	0.82	2.19	2.976(5)	160
O(4)–H(4B)…O(2)#6	0.96(5)	1.93(5)	2.885(4)	174(4)

Notes: Symmetry transformations used to generate equivalent atoms for H_2L: #1 $-x+1, -y, -z+1$; for **2**: #2 $-x+1/2, -y+1/2, z-1/2$; #3 $x+1/2, -y+1/2, -z+3/2$; for **3**: #4 $-x, y-1/2, -z+1/2$; #5 $1-x, y+1/2, -z+1/2$; #6 $-x, y+1/2, -z+1/2$.

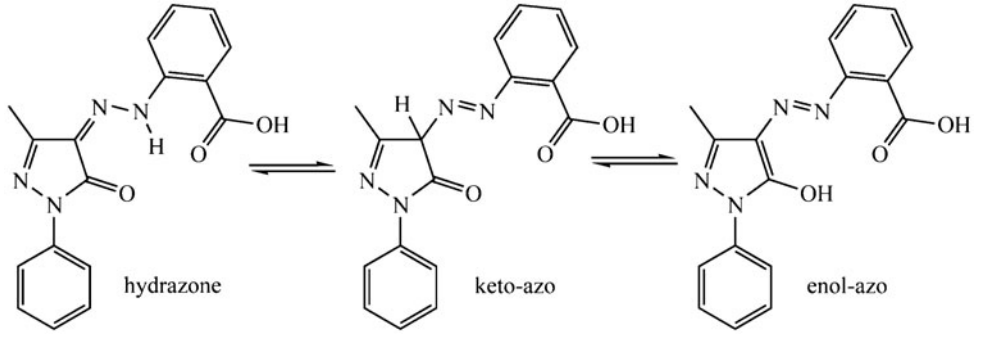

Scheme 1. The existence of different tautomeric forms in the ligand.

3.2. *Crystal structure description*

3.2.1. Structure of H_2L. The crystal structure of H_2L has not been reported. Thus, to further explore the relationship between the structure and properties, as well as to identify the possible methods of altering and controlling the structure via chemical, thermal, and other processes, the crystal structure of H_2L was elucidated. Single crystals were obtained by slow evaporation of an ethanol solution of H_2L and were characterized via single-crystal X-ray studies. These studies revealed that H_2L crystallizes in the monoclinic space group *P2(1)/c*. The crystal structure of H_2L is illustrated in figure 1(a) with an atom-numbering scheme. The existence of azo-derivatives in different tautomeric forms (scheme 1) in solid state is a well-known phenomenon, and numerous studies have been conducted to establish the geometry of these derivatives. From the crystal structure of H_2L, the ligand adopts a non-planar conformation [the torsion angles between phenyl ring1 (C1–C6) and phenyl ring2 (C11–C16) with the pyrazolone ring are 34.375(5)° and 8.458(5)°]. The least-square plane deviation of the pyrazolone ring plane is only 0.008 Å, which shows that the five atoms are almost coplanar. Therefore, the keto-azo form of the ligand can be excluded for the distorted sp^2 hybridization of C8. Furthermore, the C8–N3 bond distance is 1.309(2) Å,

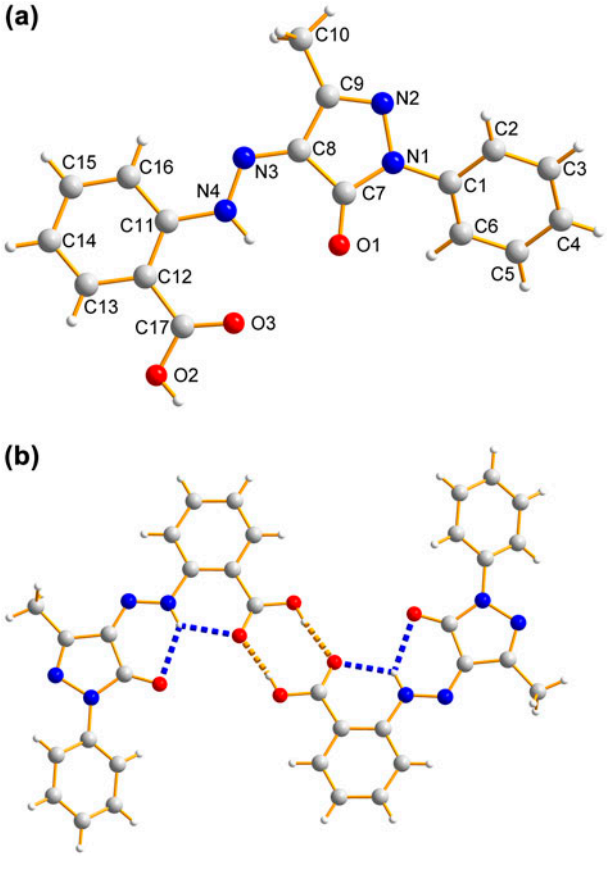

Figure 1. (a) Crystal structure of H2L with atom numbering scheme. (b) View of the dimer supported by the intra- and inter-molecular hydrogen bonds (indicated by blue and yellow dashed lines, see http://dx.doi.org/10.1080/00958972.2014.948870 for color version).

which is close to that of a C=N bond (1.309–1.331 Å) [40, 41]. This result confirms imine bond formation. Contrasted with similar reported pyrazolone compounds, the C7–O1 bond distance of 1.235(2) Å is also in accord with the value for the C=O double bond [42, 43]. Although the ligand maybe present in different forms in solution, such as hydrazo, keto-azo, and enol-azo, we can conclude that the ligand recrystallizes from ethanol solution with the hydrazone form.

In the solid state, the network of hydrogen-bond interactions, which provide extra rigidity to the ligand, has a vital role in the formation of the stabilized isomer and the packing form. The existence of the intramolecular hydrogen bonds of N4–H1…O1 and N4–H1…O3 increases the stability of the ligand by forming two six-member cheated rings. Moreover, hydrogen bonds, O2–H2B…O3#1, were observed between carboxyl groups, which connect with another molecule to form a dimer [figure 1(b)]. These intermolecular hydrogen bonds are more important to the rigidity of ligand and are stronger than the intramolecular ones.

3.2.2. Structure of $[Cu(II)L]_n$ (1). Complex **1**, which crystallized in the *C2/c* space group, is a 1-D zigzag chain polymer that is constructed by Cu(II)(μ_2-L^{2-}). The crystal structure of

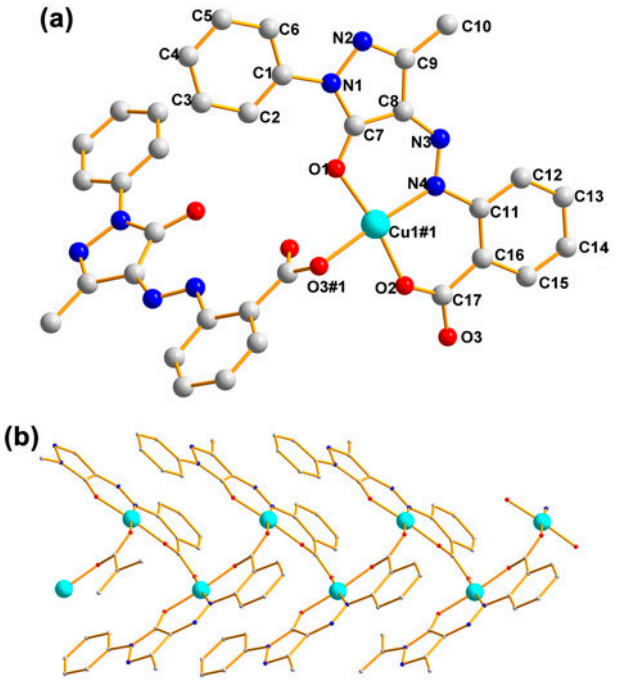

Figure 2. (a) Coordination environment of Cu(II) in **1** with atom numbering scheme; hydrogens are omitted for clarity (#1 $-x+3/2$, $y-1/2$, $-z+3/2$). (b) View of the 1-D zig–zag chain along the *b* axis in **1**.

1 is illustrated in figure 2(a) with the atom-numbering scheme. The asymmetric unit contains one crystallographically independent Cu(II) and one fully deprotonated L^{2-}. Similar to the pyrazolone ring in the crystal structure of the ligand, this ring is also nearly planar (the least-square plane deviation is 0.001 Å). The C8–N3 and C7–O1 bond lengths are shorter, whereas the N3–N4 and C7–C8 ones are longer than those in the ligand, which suggests the deprotonated tautomeric enol-azo form of the ligand. The bond lengths are intermediate between double and single bonds, thereby indicating conjugation of the delocalized π-electrons of the pyrazolone-ring and the azo bond. The Cu1#1(II) is surrounded by O1, N4, O2, and O3#1 in a distorted square planar geometry with the NO3 donor set (#1: $-x+3/2$, $y-1/2$, $-z+2/3$). The Cu–N4 (1.984(1) Å) bond length is similar to that of reported Cu–azo complexes [44, 45], which suggests that $d\pi$ (Cu) $\rightarrow \pi$ (N=N) back donation also occurred in **1**. The least-squares plane deviation of the plane with O1, N4, O2, and O3#1 is 0.028 Å, and the Cu1#1 (II) strays from the plane 0.009 Å, thereby indicating that these five atoms nearly lie in the same plane. The bond angles of O1–Cu1#1–O2 and N4–Cu1#1–O3#1 are 170.37 (11)° and 175.98(14)°, respectively, which deviate from the ideal value of 180°. The distortion of the four-coordinate complex from perfect square planar and perfect tetrahedral geometries was calculated using the τ_4 index ($\tau_4 = (360 - (\alpha + \beta)/141)$, zero is for a perfect square planar and unity for a perfect tetrahedral) [46]. τ_4 value is calculated as 0.097 for **1**. From the structural observation, we conclude that the coordination geometry around Cu(II) approximates square planar geometry.

As a tridentate ligand, the fully deprotonated ligand chelates one Cu(II) to form two almost coplanar six-membered rings with a dihedral angle of 3.637(82)°. Adjacent copper ions are connected in a *syn–anti* carboxyl bridging mode. Different from the ligand

structure, the phenyl ring1 is almost coplanar with the pyrazolone ring (the dihedral is 3.81 (17)°), which indicates the existence of a broader conjugating system in this complex. The angle between two least-square planes of the two adjacent asymmetric units is 70.11(2)° and the angle between the carboxyl and the adjacent phenyl ring is 12.01°, which results in formation of the zigzag chain [figure 2(b)].

3.2.3. Structure of $[Co(II)L]_n$ (2). Similar to those in **1**, the deprotonated tautomeric enol-azo form, which functions as a tridentate ligand in **2**, exhibits both chelating and bridging functions of the carboxyl group with a *syn–anti* mode. Single-crystal X-ray analysis reveals that **2** crystallizes in the tetragonal $I\bar{4}$ space group. The asymmetric unit of **2** comprises one distinguishable Co(II), one L^{2-}, and one water. The geometry around the Co(II) may be square pyramidal or trigonal bipyramidal depending on the geometric parameter τ_5 ($\tau_5 = (\beta - \alpha)/60$, where β is defined as the greater of the basal angles and α is the remaining angle). For a perfect square pyramidal geometry, τ is zero, whereas τ becomes unity for an ideal trigonal bipyramidal geometry [46]; τ is calculated as 0.684 for Co(II), which indicates a trigonal bipyramidal structure. As shown in figure 3(a), each Co(II) assumes a distorted trigonal bipyramidal NO4 geometry surrounded by O1 (phenolic oxygen atom), O2 (one carboxyl oxygen), O4 (one water) in the equatorial plane, and N4 (one azo nitrogen) and O3#1 (the other carboxyl oxygen) at the axial position.

In contrast to the molecular square configuration in **1**, adjacent Co(II) ions are periodically interlinked by a single-*syn–anti* carboxyl bridge into a racemic mixture of right- and left-handed $[CoII(\mu_2\text{-}L^{2-})]_n$ helical chains, running along a crystallographic $\bar{4}$ screw axis [figure 3(b)]. The carboxyl group that probably functions as the turning node to form the helical chains makes an angle of 28.92° with the adjacent phenyl ring and is bigger (16.9°) than the one in **1**. No chiral information is present in **2** because these helical chains are parallel to one another and the right- and left-handed chains are arranged alternatively [figure 3(c)].

The stability of the final helical structure lies on the O4–H4A…O2#2 intramolecular and the O4–H4A…N3#3 intermolecular hydrogen bonds. The intermolecular hydrogen bonds connect the alternating left- and right-handed helical chains, generating two different sizes of holes in **2** [figure 3(d)]. A number of helical coordination polymers with different kinds of ligands have been reported, and the more intriguing helical compounds with independent motifs that are entangled together have been synthesized and reviewed [47, 48]. Although **2** has the turning node and non-covalent interactions, the entangled metal-organic framework did not form for lack of other influencing factors [47]. Compound **2** is the first azo-pyrazolone compound that contains infinite helical chains.

3.2.4. Structure of $Ni(II)L(DMF)(H_2O)_2$ (3). To further investigate the influence of the anion on the structure of the complexes, the reactions of H_2L with three different nickel salts were carried out to obtain a coordination polymer. Unfortunately, **3** is mononuclear and its structure is depicted in figure 4(a). The Ni(II) is in a (3 + 1 + 2) surrounding and is coordinated by two oxygens (O1, O2) and one nitrogen (N4) from the fully deprotonated L^{2-} as well as one oxygen (O6) from DMF and two oxygens (O4, O5) from water to form a NiNO5 coordination environment. The deviation of Ni(II) from the equatorial plane defined by O1, O2, N4, and O6 (the mean deviation from the plane is 0.102 Å) is 0.025 Å, indicating the five atoms are almost coplanar. The Ni–O1, Ni–N4, Ni–O2, and Ni–O6 bond lengths are 1.980(2), 2.036(3), 1.974(2), and 2.099(3) Å and the bond angles of N4–Ni–O1,

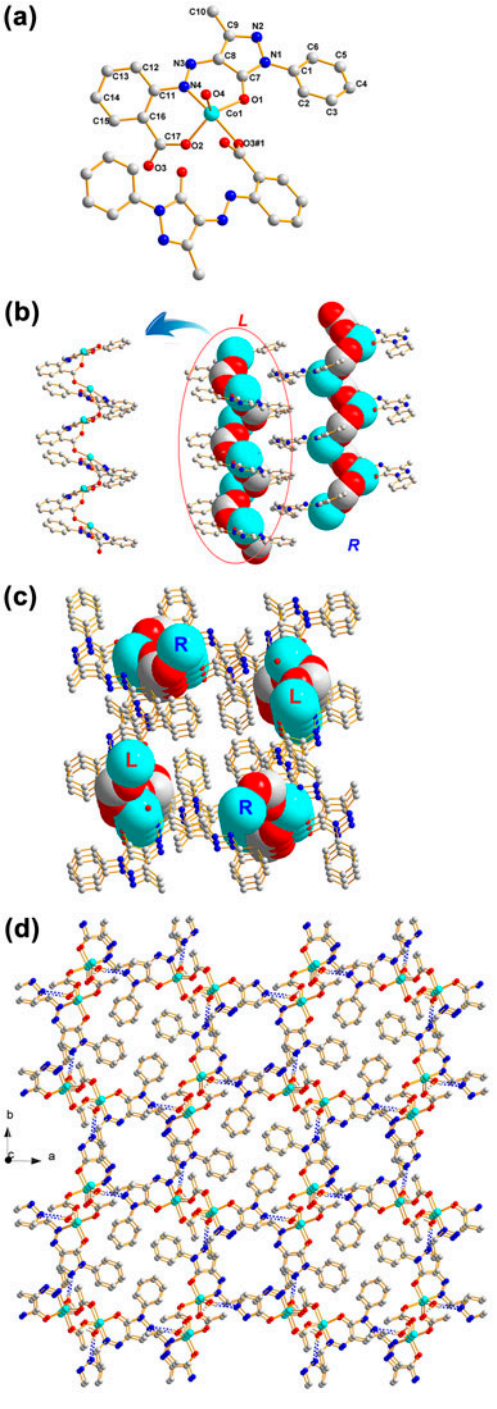

Figure 3. (a) Coordination environment of Co(II) in **2** with atom numbering scheme; hydrogens are omitted for clarity (#1 $-x+1/2, -y+1/2, z-3/2$). (b) Two types of helical chains constructed by μ_2–L_{2-} and Co(II), left-handed helix (L) and right-handed helix (R). (c) Relative position of two types of helical chains in **2**. (d) 3-D structure of **2** by linking adjacent helical chains through intermolecular hydrogen bonds indicated by dashed bonds.

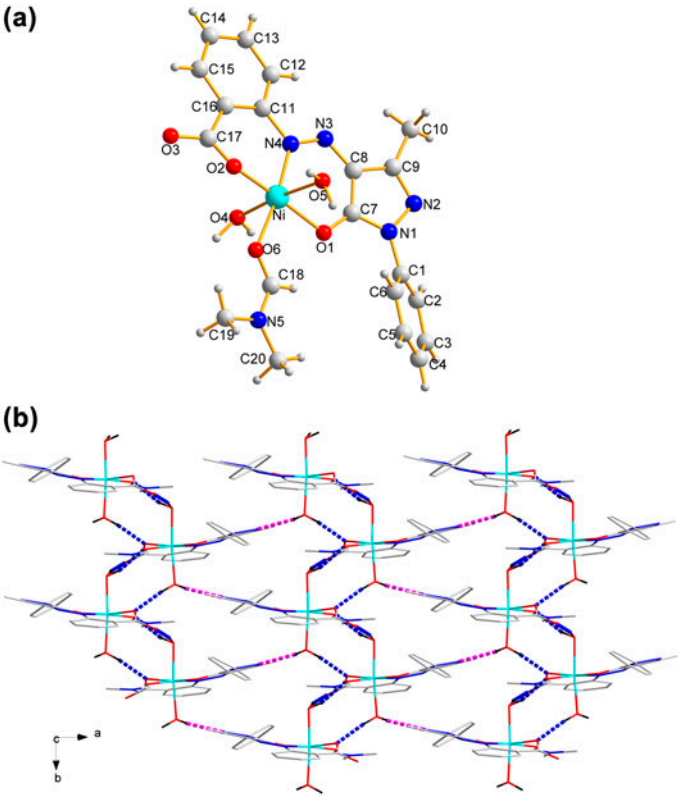

Figure 4. (a) Coordination environment of Ni(II) in **3** with atom numbering scheme. (b) 1-D chains and 2-D supermolecular supported by intermolecular hydrogen bonds (indicated by blue and purple dashed lines, respectively, see http://dx.doi.org/10.1080/00958972.2014.948870 for color version).

N4–Ni–O6, and O1–Ni–O2 are 96.58(11)°, 173.36(11)°, and 169.13(11)°, respectively. This indicates that Ni is in a distorted square plane composed of four chelating atoms. The Ni (II)–N(azo) bond length is longer than that in the literature [49], but the similarity to that in the literature [50] may be due to the coordination mode of Ni(II). O4 and O5 of two waters are located on both sides of the planar structure with long Ni–O distances (2.099(3) and 2.100(3) Å). The ligand–metal–ligand bite angles vary between 84.11(10)° [O1–Ni–O5] and 97.71(10)° [O2–Ni1–O6]. From the crystal analysis, we conclude that **3** adopts a distorted octahedral conformation.

Similar to the former two complexes, the keto form of HL loses two protons to isomerize to the enol form. In this complex, the bond length of C7–O1 is 1.264(4) Å, shorter than the C–O single bond and longer than a C=O double bond. The N3–N4 bond length is close to the N=N double bond one, indicating the enol form of the ligand. The N(1)–N(2) bond length is 1.301(4) Å, which is shorter than that in the free ligand. These changes indicate that delocalized pyrazolone rings result in averaging the bond length. Based on the X-ray analysis results, phenyl ring1 and phenyl ring2 are non-planar with the pyrazolone ring. The dihedral angles are 43.23(13)° and 10.72(16)°, respectively. Complex **3** contains two waters, which factor prominently in increasing the stability of the complex. Adjacent monomeric units are linked to form the 1-D structure through intermolecular hydrogen

bonds of O5–H5B…O3#4, O5–H5A…O6#4 and O4–H4B…O2#6 [figure 4(b)]. Thus, a 2-D supramolecular structure is generated by connecting 1-D chains through hydrogen bonds of O4–H4A…N2#5. In this case, H-bonding interactions have a vital function in forming the supramolecular structure via self-assembly and stabilization.

3.3. *PXRD patterns*

To confirm the phase purity of each compound, PXRD patterns were obtained and the results indicate that each bulk sample was a pure phase, as indicated by the experimental and simulated PXRD patterns calculated from single-crystal diffraction data (figure S2).

3.4. *Thermal analyses*

To obtain the thermal stability of **1–3**, thermal analyses were performed using TGA techniques from 50 to 700 °C (figure 5). Based on the mass losses curve, two-step decomposition is proposed for **3** with the first stage of decomposition at 92 °C and finished at 320 °C. The estimated mass loss of 21.7% in this region accounts for the elimination of lattice water and DMF (Calcd 22.4%). Similar to that reported [23], the second mass loss was observed between 320 and 431 °C, which may be attributed to elimination of $C_7H_4N_2O_2$ (expt. 29.7%, Calcd 30.3%). The remaining decomposition step with an estimated mass loss 18.1% is roughly assigned to the loss of residual ligand molecules. The total mass loss of 69.5% is less than the calculated value of 84.7% if the final product is assumed to be NiO. This result indicates that the decomposition is incomplete. The TGA profile for **2** shows that the complex was stable to 206 °C and an initial mass loss of one lattice water molecule per formula unit (expt. 3.8%, Calcd 4.5%) occurs from 206 to 260 °C. The next step with an estimated mass loss of 75.9% (Calcd 76.6%) within the temperature range of 260–700 °C corresponds to loss of ligand and was consistent with oxidative decomposition of the complex, leading to the formation of metal oxide. By contrast, **1** is thermally stable up to

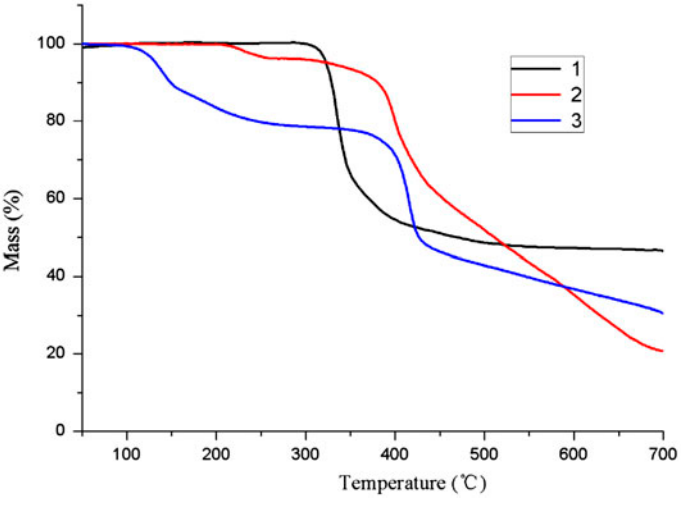

Figure 5. TG curves of **1–3**.

298 °C without any weight loss because of the absence of the small molecules in the crystal structure. The only mass loss of 47.9% was observed from 298 to 534 °C, corresponding to elimination of $C_{10}H_8N_4O_1$ (Calcd 48.3%). These thermal data show that **1** is thermally more stable than **2** and **3**.

3.5. *Fluorescent properties*

The fluorescence spectra of H_2L, **1**, **2**, and **3** were measured in the solid state at room temperature. As shown in figure 6, the free ligand shows two main emission peaks at 470 and 590 nm upon excitation at 360 nm. One similar peak (470 nm) and one blueshift (540 nm) emission were observed in **1**, compared with that in H_2L. The similar emission is probably due to the intraligand charge transfer (ILCT) fluorescent emission, which is a previously reported phenomenon [51–54]. The blueshift band at 540 nm compared with that of the free H_2L ligand at 570 nm may be due to the chelating of the ligand-to-metal charge transfer (LMCT), which increases the rigidity of the ligand and reduces the loss of energy via radiationless decay of the intraligand emission-excited state [55–57]. Therefore, these results predict that the emissive excited state of **1** is primarily attributed to the ILCT plus LMCT state [58, 59]. Upon chelation of H_2L with Cu(II), Co(II), and Ni(II), the intensities of emissions decreased to varying extents, and almost 100% fluorescence emission quenching was observed in **2** and **3**. The metal centers in **1–3** should be electron-deficient and accept the electron or energy transferred from the excited state of H_2L, thereby providing efficient fluorescence attenuation for H_2L [60]. More small molecules were found in **3** (two H_2O and one DMF) than in **1** and **2** (no small molecule and one H_2O, respectively), which provide an efficient pathway for quenching the fluorescence via an energy or electron transfer [34]. Coordination of Co(II) and Ni(II) with the ligand decreased the rigidity of the two 1-D complexes, which may lead to fluorescence attenuation [61, 62].

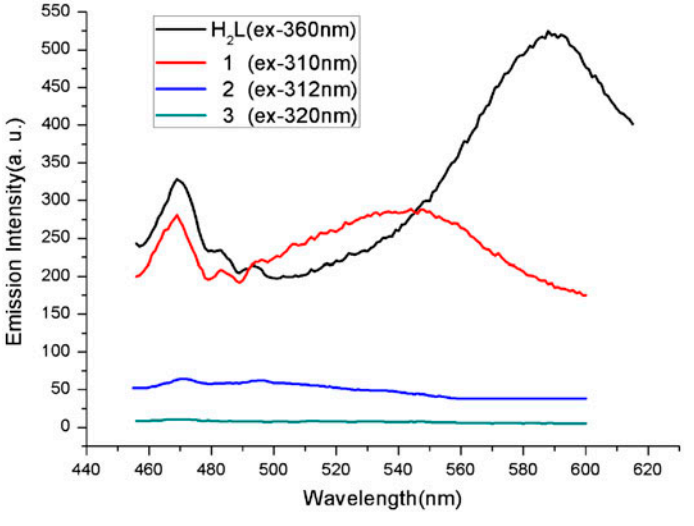

Figure 6. The fluorescence spectra of H2L and **1**–**3**.

4. Conclusion

Three new complexes with pyrazolone-based azo-ligand were synthesized and structurally characterized. Complex **2** is the first helical structure with pyrazolone-based azo-ligand. The left- and right-helical chains are connected by intra- and intermolecular hydrogen bonds to generate a 3-D framework with two different sizes of holes. The fluorescence proved that only the Cu(II) complex can emit fluorescence, which may be useful in distinguishing the Cu(II) cation from Co(II) and Ni(II).

Supplementary material

PXRD graphics and solid-state IR spectra of H_2L, and **1–3** are available as supplementary material. CCDC 949716, 949717, 949718, and 949719 contain the supplementary crystallographic data for H_2L, **1**, **2**, and **3** in this paper. These data can be obtained free of charge from the Cambridge Crystallographic Data Center via www.ccdc.cam.ac.uk/data_request/cif.

Funding

This work was supported by the National Natural Science Foundation of China (Projects 21061016 and 21371151) and Yunnan Provincial Department of Education Research Fund (Project 2011Y111).

References

[1] Y.-Z. Zheng, Z.-P. Zheng, X.-M. Chen, S.-M. Fang. *Coord. Chem. Rev.*, **257**, 1282 (2013).
[2] F. Novio, J. Simmchen, N. Vázquez-Mera, L. Amorín-Ferré, D. Ruiz-Molina. *Coord. Chem. Rev.*, **257**, 2839 (2013).
[3] X.-Q. Zhao, P. Cui, B. Zhao, W. Shi, P. Cheng. *Dalton Trans.*, 805 (2011).
[4] Z.-M. Man, F. Guo. *J. Coord. Chem.*, **66**, 1 (2013).
[5] M. Du, C.-P. Li, C.-S. Liu, S.-M. Fang. *Coord. Chem. Rev.*, **257**, 1282 (2013).
[6] T.R. Cook, Y.-R. Zheng, P.J. Stang. *Chem. Rev.*, **113**, 734 (2012).
[7] G. Kumar, R. Gupta. *Chem. Soc. Rev.*, **42**, 9403 (2013).
[8] Y.-L. Lu, W.-J. Zhao, X. Feng, Y. Chai, Z. Wu, X.-W. Yang. *J. Coord. Chem.*, **66**, 473 (2013).
[9] Q. Huang, W. Tang, C. Liu, X. Su, X. Meng. *J. Coord. Chem.*, **67**, 149 (2014).
[10] R.K. Vakiti, B.D. Garabato, N.P. Schieber, M.J. Rucks, Y. Cao, C. Webb, J.B. Maddox, A. Celestian, W.-P. Pan, B.-B. Yan. *Cryst. Growth Des.*, **12**, 3937 (2012).
[11] R. Horikoshi, T. Mochida. *Eur. J. Inorg. Chem.*, **34**, 5355 (2010).
[12] M. Andruh. *Chem. Commun.*, **47**, 3025 (2011).
[13] H.-Y. Chen, D.-R. Xiao, S.-W. Yan, J.-H. He, J. Yang, X. Wang, E.-B. Wang. *Inorg. Chim. Acta*, **387**, 283 (2012).
[14] G. Li, Y. Chen, J. Han, H. Ye, X. Wang, T. Wang. *Dyes Pigm.*, **94**, 314 (2012).
[15] R. Ebdelli, A. Rouis, R. Mlika, I. Bonnamour, H. Ben Ouada, J. Davenas. *J. Mol. Struct.*, **1006**, 210 (2011).
[16] B.A. Yamgar, V.A. Sawant, B.G. Bharate, S.S. Chavan. *Spectrochim. Acta, Part A*, **78**, 102 (2011).
[17] X.-W. Tan, X.-H. Xie, J.-Y. Chen, S.-Z. Zhan. *Inorg. Chem. Commun.*, **13**, 1455 (2010).
[18] M.S. Masoud, S.S. Hagagg, A.E. Ali, N.M. Nasr. *J. Mol. Struct.*, **1014**, 17 (2012).
[19] A.R. Kennedy, H. Stewart, K. Eremin, J. Stenger. *Chem. Eur. J.*, **18**, 3064 (2012).
[20] D.-Q. Zhang, W.-S. Jin. *Spectrochim. Acta, Part A*, **90**, 35 (2012).
[21] G.-Q. Zhang, S.-Q. Wang, J.-S. Ma, G.-Q. Yang. *Inorg. Chim. Acta*, **384**, 97 (2012).
[22] Z. Chen, F. Huang, Y. Wu, D. Gu, F. Gan. *Inorg. Chem. Commun.*, **9**, 21 (2006).
[23] X. Li, Y. Wu, D. Gu, F. Gan. *Dyes Pigm.*, **86**, 182 (2010).
[24] R.N. Jadeja, K.M. Vyas, V.K. Gupta, R.G. Joshi, C. Ratna Prabha. *Polyhedron*, **31**, 767 (2012).
[25] M.-F. Wang, Z.-Y. Yang, Y. Li, H.-G. Li. *J. Coord. Chem.*, **64**, 2974 (2011).
[26] W.-L. Jiang, B. Lou, J.-Q. Wang, H.-B. Lv, Z.-Q. Bian, C.-H. Huang. *Dalton Trans.*, 11410 (2011).

[27] C. Pettinari, F. Marchetti, I. Timokhin, A. Marinelli, C. Di Nicola, B.W. Skelton, A.H. White. *Inorg. Chim. Acta*, **367**, 98 (2011).
[28] H.-Z. Wu, T.-S. Yang, Q. Zhao, J. Zhou, C.-Y. Li, F.-Y. Li. *Dalton Trans.*, 1969 (2011).
[29] G.-C. Xu, L. Zhang, Y.-H. Zhang, J.-X. Guo, M.-Q. Shi, D.-Z. Jia. *CrystEngComm*, **15**, 2873 (2013).
[30] H. Li, G.-C. Xu, L. Zhang, J.-X. Guo, D.-Z. Jia. *Polyhedron*, **55**, 209 (2013).
[31] J. Zhou, L. Du, Z.-Z. Li, Y.-F. Qiao, J. Liu, M.-R. Zhu, P. Chen, Q.-H. Zhao. *J. Coord. Chem.*, **66**, 2166 (2013).
[32] E. Colacio, M. Ghazi, R. Kivekäs, J.M. Moreno. *Inorg. Chem.*, **39**, 2882 (2000).
[33] X.-Y. Zhang, Z.-Y. Liu, Y.-F. Xia, Y.-Y. Zhang, E.-C. Yang, X.-J. Zhao. *J. Coord. Chem.*, **66**, 4399 (2013).
[34] Z.-Z. Li, L. Du, J. Zhou, M.-R. Zhu, F.-H. Qian, J. Liu, Q.H. Zhao. *Dalton Trans.*, 14397 (2012).
[35] J. Zhou, L. Du, Z.-Z. Li, Y.-F. Qiao, J. Liu, M.-R. Zhu, P. Chen, Y. Hu, Q.-H. Zhao. *Polyhedron*, **54**, 252 (2013).
[36] K. Nejati, Z. Rezvani, E. Alizadeh, R. Sammimi. *J. Coord. Chem.*, **64**, 1859 (2011).
[37] G.M. Sheldrick. *Program for Empirical Absorption Correction of Area Detector Data*, University of Göttingen, Germany (1996).
[38] G.M. Sheldrick. *SHELX-97, Programs for the Solution of Crystal Structures*, University of Göttingen, Germany (1997).
[39] G.M. Sheldrick. *SHELX-97, Programs for the Refinement of Crystal Structures*, University of Göttingen, Germany (1997).
[40] M.N. Kopylovich, K.T. Mahmudov, M. Haukka, K.V. Luzyanin, A.J. Pombeiro. *Inorg. Chim. Acta*, **374**, 175 (2011).
[41] K.T. Mahmudov, M.N. Kopylovich, K.V. Luzyanin, A. Mizar, M.F.C. Guedes da Silva, V. André, A.J.L. Pombeiro. *J. Mol. Struct.*, **992**, 72 (2011).
[42] B.-H. Peng, G.-F. Liu, L. Liu, D.-Z. Jia, K.-B. Yu. *J. Mol. Struct.*, **692**, 217 (2004).
[43] Y. Kamei, H. Shibata, J. Mizuguchi. *J. Imaging Sci. Technol.*, **55**, 30508 (2011).
[44] K. Pramanik, M. Sekhar Jana, T.K. Mondal. *J. Coord. Chem.*, **66**, 4067 (2013).
[45] X.-W. Tan, X.-H. Xie, J.-Y. Chen, S.-Z. Zhan. *Inorg. Chem. Commun.*, **13**, 1455 (2010).
[46] L. Yang, D.R. Powell, R.P. Houser. *Dalton Trans.*, 955 (2007).
[47] G.-P. Yang, L. Hou, X.-J. Luan, B. Wu, Y.-Y. Wang. *Chem. Soc. Rev.*, **41**, 6992 (2012).
[48] Z.-G. Gu, X.-X. Xu, W. Zhou, C.-Y. Pang, F.-F. Bao, Z. Li. *Chem. Commun.*, **48**, 3212 (2012).
[49] Z.-M. Yin, Y. Yan, S.-P. Sun, W.-Y. Wang. *J. Coord. Chem.*, **65**, 865 (2012).
[50] M.N. Kopylovich, M.F.C.G. Guedes da Silva, L.M.D.R.S. Martins, M.L. Kouznetsov, K.T. Mahmudov, A.J. Pombeiro. *Polyhedron*, **50**, 374 (2013).
[51] Q.-Q. Liang, Z.-Y. Liu, E.-C. Yang, X.-J. Zhao. *Z. Anorg. Allg. Chem.*, **635**, 2653 (2009).
[52] M.-F. Wang, X.-J. Hong, Q.-G. Zhan, H.-G. Jin, Y.-T. Liu, Z.-P. Zheng, S.-H. Xu, Y.-P. Cai. *Dalton Trans.*, 11898 (2012).
[53] W. Xu, F. Jiang, Y. Zhou, K. Xiong, L. Chen, M. Yang, R. Feng, M. Hong. *Dalton Trans.*, 7737 (2012).
[54] L. Li, J. Zhao, C. Wang, S. Yang, H. Hou. *Z. Anorg. Allg. Chem.*, **638**, 187 (2012).
[55] X.-L. Wang, Y.-F. Bi, H.-Y. Lin, G.-C. Liu. *Cryst. Growth Des.*, **7**, 1086 (2007).
[56] L. Wang, W. Gu, J.-X. Deng, M.-L. Liu, N. Xu, X. Liu. *Z. Anorg. Allg. Chem.*, **636**, 1124 (2010).
[57] R. Sun, Y.-Z. Li, J. Bai, Y. Pan. *Cryst. Growth Des.*, **7**, 890 (2007).
[58] L.-P. Zhang, L.-G. Zhu. *Z. Anorg. Allg. Chem.*, **634**, 39 (2008).
[59] Z.-L. Fang, J.-G. He, R.-M. Yu, X.-Y. Wu, C.-Z. Lu. *CrystEngComm*, **13**, 6243 (2011).
[60] Z. Huang, J. Du, J. Zhang, X.-Q. Yu, L. Pu. *Chem. Commun.*, **48**, 3412 (2012).
[61] P.-P. Yang, B. Li, Y.-H. Wang, W. Gu, X. Liu. *Z. Anorg. Allg. Chem.*, **634**, 1221 (2008).
[62] H.-H. Zhang, W. Dou, W.-S. Liu, X.-L. Tang, W.-W. Qin. *Eur. J. Inorg. Chem.*, **5**, 748 (2011).